Received: 13 December 2017 | Revised: 14 May 2018 | Accepted: 20 May 2018

DOI: 10.1002/nbm.3961

RESEARCH ARTICLE

WILEY NMR IN BIOMEDICINE

# Quantitative evaluation of pulmonary gas-exchange function using hyperpolarized $^{129}$Xe CEST MRS and MRI

Haidong Li[1,2] | Zhiying Zhang[1,2] | Xiuchao Zhao[1,2] | Yeqing Han[1,2] | Xianping Sun[1,2] | Chaohui Ye[1,2] | Xin Zhou[1,2]

[1] State Key Laboratory of Magnetic Resonance and Atomic and Molecular Physics, National Center for Magnetic Resonance in Wuhan, Wuhan Institute of Physics and Mathematics, Chinese Academy of Sciences, Wuhan, China

[2] University of Chinese Academy of Sciences, Beijing, China

**Correspondence**
Xin Zhou, PhD, Wuhan Institute of Physics and Mathematics, Chinese Academy of Sciences, 30 West Xiaohongshan, Wuhan, China.
Email: xinzhou@wipm.ac.cn

**Funding information**
Key Research Program of Frontier Sciences, CAS, Grant/Award Number: QYZDY-SSW-SLH018; National Key R&D Program of China, Grant/Award Numbers: 2016YFC1304700 and 2017YFA0505400; National Natural Science Foundation of China, Grant/Award Numbers: 81625011, 81227902 and 81601491; National Program for Support of Eminent Professionals (National Program for Support of Top-notch Young Professionals)

Hyperpolarized $^{129}$Xe gas MR has been a powerful tool for evaluating pulmonary structure and function due to the extremely high enhancement in spin polarization, the good solubility in the pulmonary parenchyma, and the excellent chemical sensitivity to its surrounding environment. Generally, the quantitative structural and functional information of the lung are evaluated using hyperpolarized $^{129}$Xe by employing the techniques of chemical shift saturation recovery (CSSR) and xenon polarization transfer contrast (XTC). Hyperpolarized $^{129}$Xe chemical exchange saturation transfer (Hyper-CEST) is another method for quantifying the exchange information of hyperpolarized $^{129}$Xe by using the exchange of xenon signals according to its different chemical shifts, and it has been widely used in biosensor studies in vitro. However, the feasibility of using hyperpolarized $^{129}$Xe CEST to quantify the pulmonary gas exchange function in vivo is still unclear. In this study, the technique of CEST was used to quantitatively evaluate the gas exchange in the lung globally and regionally via hyperpolarized $^{129}$Xe MRS and MRI, respectively. A new parameter, the pulmonary apparent gas exchange time constant ($T_{app}$), was defined, and it increased from 0.63 s to 0.95 s in chronic obstructive pulmonary disease (COPD) rats (induced by cigarette smoke and lipopolysaccharide exposure) versus the controls with a significant difference ($P$ = 0.001). Additionally, the spatial distribution maps of $T_{app}$ in COPD rats' pulmonary parenchyma showed a regionally obvious increase compared with healthy rats. These results indicated that hyperpolarized $^{129}$Xe CEST MR was an effective method for globally and regionally quantifying the pulmonary gas exchange function, which would be helpful in diagnosing lung diseases that are related to gas exchange, such as COPD.

**KEYWORDS**

CEST, cigarette smoke, COPD, gas exchange function, hyperpolarized xenon, lung

## 1 | INTRODUCTION

Hyperpolarized noble gas MR is a powerful tool for evaluating pulmonary structure and functional information due to the extremely high enhancement in spin polarization using the technique of spin-exchange optical pumping.[1-5] Among the candidates for hyperpolarized noble gas MR, i.e. $^{3}$He, $^{129}$Xe, and $^{83}$Kr, $^{129}$Xe has unique advantages for the exploration of the pulmonary gas exchange function because of its good solubility

**Abbreviations used:** CEST, chemical exchange saturation transfer; COPD, chronic obstructive pulmonary disease; CSSR, chemical shift saturation recovery; CW, continuous wave; FWHM, full width at half maximum; LPS, lipopolysaccharide; MOXE, model of xenon exchange; SNR, signal-to-noise ratio; $T_{app}$, the pulmonary apparent gas exchange time constant; XTC, xenon polarization transfer contrast

  

in the pulmonary parenchyma and excellent chemical sensitivity to its surrounding environment.[4,6-8] Recently, many studies have demonstrated the feasibility of hyperpolarized $^{129}$Xe MR for exploring the pulmonary gas-blood exchange function.[9-13]

Pulmonary gas exchange functional parameters are generally extracted from the dynamics of dissolved xenon signals versus the gas exchange time. The dynamics of dissolved xenon in the lung can be obtained either directly by measuring dissolved xenon signals, which is called chemical shift saturation recovery (CSSR), or indirectly by measuring the gaseous xenon signal of the alveoli, which was first proposed by Ruppert and colleagues and is called xenon polarization transfer contrast (XTC).[11,14,15] By using a corresponding theoretical pulmonary gas exchange model, such as the Patz model,[12] Mansson model,[2] or model of xenon exchange (MOXE),[16] among others,[17,18] the quantitative pulmonary structure and functional parameters, such as the gas exchange time, thickness of the alveolar barrier, surface to volume ratio, and so on, can be obtained.[11,19] In recent years, the CSSR technique has been widely utilized to explore the gas exchange function in fibrosis, chronic obstructive pulmonary disease (COPD), radiation-induced lung injury, and so on.[2,9,20,21] Additionally, some groups have succeeded in directly acquiring dissolved xenon MRI of the lung tissue and blood and evaluated the distributions of the gas exchange function changes in the lungs.[3,13,22,23] Unlike the CSSR technique, XTC employs a gaseous xenon signal in the alveoli to amplify the weak dissolved xenon signals in the parenchyma, which are only approximately 2% of the gaseous $^{129}$Xe signal.[24] Therefore, the spin polarization of xenon in XTC does not need to be as high as that in the direct-detection method (CSSR). XTC has been widely used to quantitatively and regionally evaluate pulmonary structure and function.[12,17,18,25]

Hyperpolarized xenon chemical exchange saturation transfer (Hyper-CEST), as proposed by Schröder and colleagues, is another indirect-detection method that is generally utilized in hyperpolarized xenon MR and has been widely used in hyperpolarized xenon biosensor studies.[26-28] Hyper-CEST uses the exchange of xenon signals according to different chemical shifts to quantify exchange information, which is similar to XTC, but instead of the exchange time, the saturation time is variable in Hyper-CEST. On the basis of these characteristics, it was hypothesized that the pulmonary gas exchange function could be quantified by hyperpolarized xenon CEST MR.

In this study, we demonstrated the feasibility of chemical exchange saturation transfer (CEST) using hyperpolarized xenon MR to quantify the pulmonary gas exchange function. A new parameter, the pulmonary apparent gas exchange time constant ($T_{app}$), which is closely related to gas exchange, was proposed to characterize the pulmonary gas exchange function using hyperpolarized xenon MR spectroscopy and imaging. $T_{app}$ in healthy rats and COPD rats induced by cigarette smoke and lipopolysaccharide (LPS) exposure was quantified. In addition, the regional distributions of $T_{app}$ in the lungs were also mapped.

## 2 | MATERIALS AND METHOD

### 2.1 | Hyperpolarized xenon preparation and delivery

Hyperpolarized xenon gas was produced via spin-exchange optical pumping using a homebuilt polarizer.[29-31] The polarizer was equipped with a 75 W narrow-width laser array (QPC Laser, Sylmar, CA, USA) and worked in continuous-flow mode, and the source gas mixture consisted of 1% natural abundance xenon (26.4% $^{129}$Xe), 10% $N_2$, and 89% $^4$He. After polarization, xenon was separated by flowing through a glass trap immersed in a liquid nitrogen bath placed in a 2000 Gauss magnetic field. Xenon accumulated as a solid, while the other gases flowed through. The flow rate was 0.5 standard liters per minute. Following approximately 1 h accumulation, solid xenon was thawed with hot water into gas and then stored in a Tedlar bag. The available polarization for the MR experiments was approximately 15%.

The Tedlar bag containing the hyperpolarized xenon was connected to a homebuilt MRI-compatible xenon gas delivery system.[32-34] The delivery system can deliver hyperpolarized xenon gas and oxygen to rats' lungs alternately according to the requirements of the experiments through solenoid and pneumatic valves, which were controlled by a homebuilt LabVIEW program using an NI acquisition card (National Instruments, Austin, TX, USA). The delivery system can also monitor the pressure in the rat lung in real time and trigger the MRI scanner.

### 2.2 | Animal preparation

All animal handling protocols were approved by the institutional animal care committee. Six Sprague Dawley rats were exposed to cigarette smoke for one month (twice a day, 30 min each time) before the MR experiments. On the first and 14th days, LPS was administered by endotracheal instillation at a dose of 1 mg/kg to accelerate the severity of injury.[35,36] Another six healthy SD rats served as the control group. Rats were ventilated with xenon and oxygen alternately through a 14-gauge catheter controlled by a homebuilt MRI-compatible delivery system during the experiments. A 5% isoflurane and 95% oxygen gas mixture was used during the intubation surgery, and 1.5% isoflurane was used for maintenance. Rats were sacrificed by an anesthetic overdose after the experiments.

### 2.3 | MR data acquisition

All of the MR experiments were performed on a Bruker BioSpec 4.7 T MRI system using a horizontal, 30 cm bore magnet (Oxford Instruments, Oxford, UK) equipped with a 200 mT/m shielded gradient (B-GA12S). The data were collected using a homebuilt dual-tuned birdcage coil, which was tuned to the $^1$H and $^{129}$Xe resonances (200.29 MHz and 55.4 MHz, respectively). The pulse sequence for measuring the dissolved xenon dynamics of the lung is shown in Figure 1. To eliminate the possible instability of the xenon signal caused by relaxation or other occasional factors,

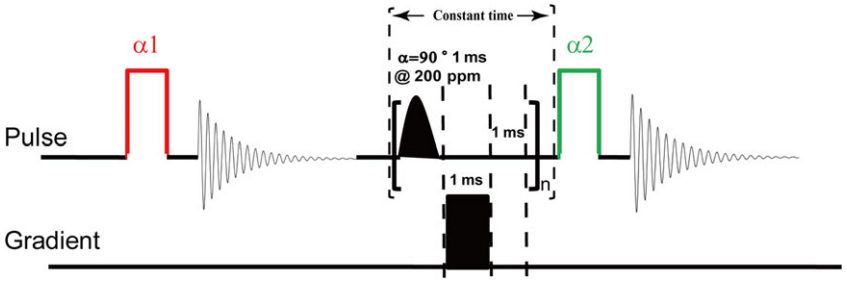


**FIGURE 1** Schematic diagram of the pulse sequence for measuring the dissolved xenon dynamics of the lung. Two excitation RF pulses were utilized. The first excitation pulse was used to acquire a reference signal, and the second one was used to generate the xenon signal. Between the two RF excitation pulses, a series of saturation pulses (Gaussian shaped, 1 ms duration, 90 degrees) were used to saturate the dissolved xenon signal in the lung to acquire the xenon gas signal decay dynamics. Following each saturation pulse, a 1 ms gradient pulse was applied to destroy the residual magnetism, and a 1 ms delay was added because of the scanner's limitation. The time between the first saturation pulse and second excitation pulse was constant, 3000 ms in this study

two excitation RF pulses with a rectangular-shaped envelope centered on gas phase resonance were used during each acquisition. The first excitation RF pulse with a flip angle of $\alpha_1$ (less than 10 degrees) was used as a reference to calibrate the xenon signal of the lung, and the second excitation pulse with a flip angle of $\alpha_2$ (90 degrees) was used for acquiring the xenon signal. Between the two excitation pulses, a series of saturation pulses (frequency-selective, Gaussian-shaped RF pulses) centered at 200 ppm (relative to a gas phase chemical shift of 0 ppm) with a duration of 1 ms was applied to saturate the dissolved xenon signals. Following each saturation pulse, a spoiler gradient pulse with duration of 1 ms was applied to destroy the residual transversal magnetism. Because of the scanner's limitation, a delay of 1 ms was added between the saturation pulses to execute the sequence. To achieve hyperpolarized $^{129}$Xe signal dynamics of the lung as a function of the saturation time, the number of saturation pulses varied from 50 to 1000. The interval between the first saturation pulse and second excitation pulse was set to a constant, 3000 ms in this study, to avoid any influence of relaxation on different acquisitions with varied saturation times. Before CEST data collection, a control experiment was implemented to calibrate the influence of relaxation and RF pulses' off-resonance, with the saturation RF pulses centered at −200 ppm. All of the MR spectra were acquired with a bandwidth of 25 kHz and 1024 sampling points, and the acquisition time for each spectroscopy was about 3.1 s. The MR data were acquired during a breath-hold (3500 ms) after rats inhaled hyperpolarized xenon gas for the second time, and the lung pressure was 12 cm $H_2O$ during the breath-hold in each experiment. The breath-hold of the rat was maintained by a homebuilt gas delivery system through solenoid and pneumatic valves, which were controlled by a homebuilt LabVIEW program using an NI acquisition card.[32-34] Sixteen xenon breath-holds were required for each rat to accomplish one set of Hyper-CEST data collection and five oxygen breaths were inserted between the xenon breaths.

For the imaging experiments, the fast low-angle shot pulse sequence was utilized. The excitation RF pulses for the imaging sequence were centered on the gas-phase resonance. Before data acquisition, 100 RF saturation pulses (Gaussian shape, 1 ms duration, flip angle 90 degrees) were applied, with a 1 ms spoiler gradient pulse and delay of 1 ms following each pulse. These saturation pulses were centered at either 200 ppm (CEST experiment) or − 200 ppm (control experiment). The pulse sequence parameters for imaging included TR/TE, 10 ms/4 ms, flip angle 7 degrees, field of view 5 cm ×5 cm, matrix 96 ×96, slice thickness 30 mm, and acquisition time about 1.3 s. The CEST image and control image were acquired in separate xenon breath-holds, and the CEST image was acquired first. Five oxygen breaths were inserted between the xenon breaths as in the spectroscopy experiments. To optimize the SNR (signal-to-noise ratio) of the gaseous xenon signal, the lungs were flushed with hyperpolarized xenon once. Then, the image data were acquired during the breath-hold after the rats inhaled xenon for a second time. The $^{129}$Xe CEST MRI was performed on all 12 rats before the MRS experiment.

## 2.4 | Data processing

The integral of each xenon gas spectrum, which was used as the signal intensity, was calculated in TopSpin 2.0 after Fourier transformation and phase correction. The xenon signal was first calibrated using the corresponding reference data. Then, the calibrated signal was normalized according to the control signal, with the saturation pulse centered at −200 ppm. Finally, the normalized data were fitted to the mono-exponential function to extract $T_{app}$:

$$S(t) = S_0 * e^{-t*n/T_{app}} \quad (1)$$

where $S(t)$ is the normalized xenon gas signal of the lung, $S_0$ is the initial normalized xenon signal, $t$ is the delay between saturation pulses, and $n$ is the number of saturation pulses. $T_{app}$ was defined as the time xenon takes to transfer into the tissue and blood, which reflects the efficiency of the alveolar gas exchange function and depends on the speed of xenon gas diffusion into the pulmonary parenchyma. $T_{app}$ increases when the gas exchange efficiency of the alveoli decreases.

The MRI data were processed in MATLAB (MathWorks, Natick, MA, USA). All images were generated from *k*-space data using a 2D discrete Fourier transform, and no filtering was applied. The control image was used to generate a lung binary mask without background noise by image segmentation. Then, the resulting binary mask was applied to the CEST image. $T_{app}$ distribution in the image was calculated point by point with the following equation:

$$T_{app} = -t * n / \ln\left(\frac{S_{CEST}}{S_{control}}\right) \quad (2)$$

where $S_{CEST}$ and $S_{control}$ are the signal intensities in the corresponding CEST image and control image, respectively, $t$ is the delay between saturation RF pulses, equal to 3 ms, and $n$ is the number of saturation RF pulses, which is 100 in this study.

Statistical analysis was performed on all the data (including the histological data shown in the following) to assess the statistical significance between the COPD and control groups using an independent samples $t$ test by PASW Statistics 18 (SPSS, Chicago, IL, USA).

### 2.5 | Histology

After the MR experiments, the rat lungs were extracted and filled to an airway pressure of 25 cm $H_2O$ with a 4% paraformaldehyde solution for 30 min, after which they were stored in the same solution for more than 48 h and then embedded in paraffin. The sequential sections, each with a thickness of 5 μm, were stained with hematoxylin and eosin (H&E) to assess histological changes by analyzing the images acquired using a microscope (Nikon Eclipse Ts 100, Nikon Corporation, Tokyo, Japan). Image-Pro Plus software (Media Cybernetics, Rockville, MD, USA) was used to compute the alveolar diameter in each rat.

## 3 | RESULTS

### 3.1 | MRS experiments

The xenon gas signal in the lung, which was calibrated by the corresponding reference signal, was plotted against the saturation time, as shown in Figure 2. The results from the control experiment, in which the saturation pulses were centered at −200 ppm, showed that the data was more stable after calibration by the reference signal and that the signal in the lung was almost constant with increasing saturation time, as shown in Figure 2B. The xenon gas signal in the lung decreased with increasing saturation time in both healthy rats and COPD rats in the CEST experiments. Additionally, the xenon signal decayed faster in healthy rats than in COPD rats. The fitting results of the xenon signal in healthy and COPD lungs versus the saturation time are shown in Figure 2C and D, respectively.

$T_{app}$ was calculated from the dynamics of the xenon signal in the lung using Equation (1). The mean $T_{app}$ values in COPD and healthy rats were 0.95 ± 0.14 s and 0.63 ± 0.06 s, respectively. $T_{app}$ significantly increased ($P$ = 0.001) in the COPD rats. The comparison of $T_{app}$ values between the two groups is shown in Figure 3, and the measured $T_{app}$ for each rat is summarized in Table 1.

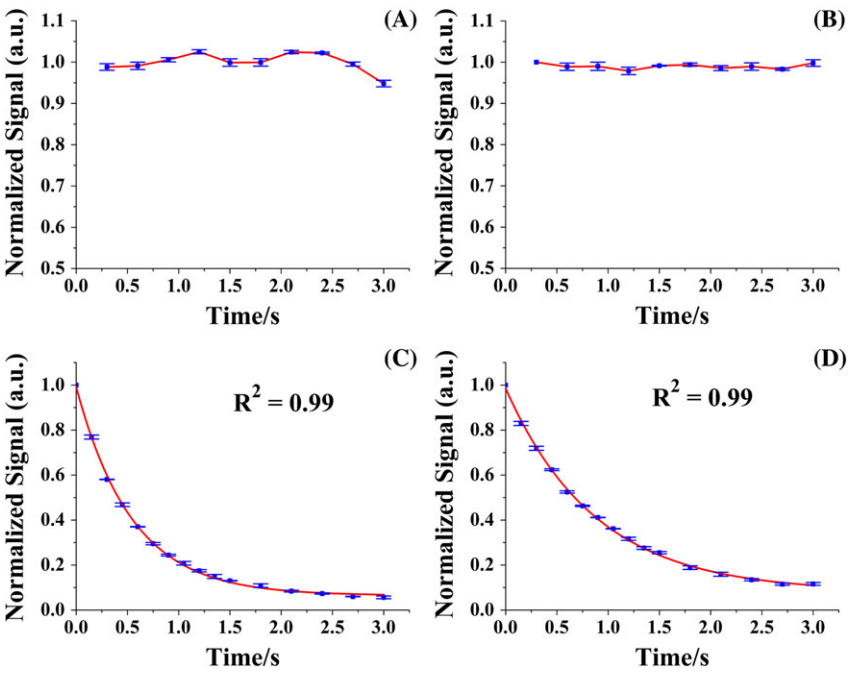


**FIGURE 2** The hyperpolarized xenon signal in the lung plotted against the saturation time. Results without and with calibration using a reference signal were shown in A and B, respectively. The reference signal was from the control experiment with the saturation pulses at −200 ppm. The xenon signals in the lung were almost constant with increasing saturation time, as shown in B. The signal decayed with increasing saturation time in the CEST experiments, in which the saturation RF pulses were centered on the resonance of the dissolved xenon signal, and the signal decayed faster in the healthy rats (C) than in the COPD rats (D)

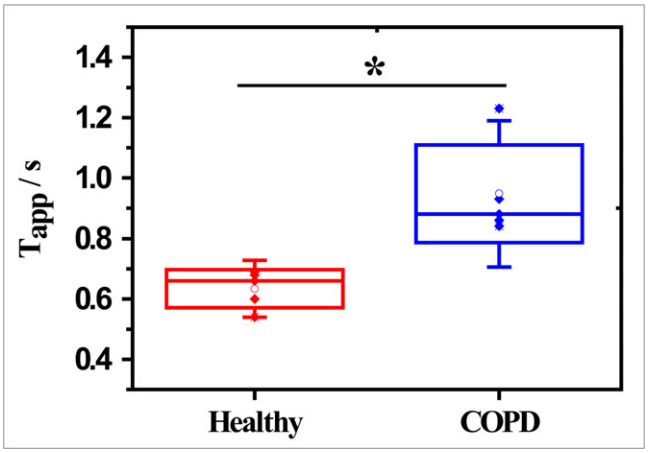


**FIGURE 3** The distribution of $T_{app}$ in both groups of rats. Each solid diamond represents the $T_{app}$ value for one rat, and the line in the middle of each box plot represents the median of each group. The hollow circle in the middle of the box plot is the mean value in each group

**TABLE 1** The measured global $T_{app}$ in healthy rats and COPD rats. The mean $T_{app}$ showed a significant difference between the groups

| | COPD | | Healthy |
|---|---|---|---|
| **Rat 1** | 1.23 ± 0.01 | **Rat 1** | 0.66 ± 0.02 |
| **Rat 2** | 0.88 ± 0.04 | **Rat 2** | 0.68 ± 0.02 |
| **Rat 3** | 0.86 ± 0.03 | **Rat 3** | 0.54 ± 0.01 |
| **Rat 4** | 0.84 ± 0.02 | **Rat 4** | 0.60 ± 0.01 |
| **Rat 5** | 0.93 ± 0.03 | **Rat 5** | 0.69 ± 0.01 |
| **Rat 6** | 0.98 ± 0.02 | **Rat 6** | 0.67 ± 0.04 |
| **Mean ± SD** | **0.95 ± 0.14** | | **0.63 ± 0.06** |
| ***p*-value** | **0.001** | | |

The unit is seconds.

## 3.2 | CEST MRI experiments

The typical $T_{app}$ distribution maps acquired from healthy rats and COPD rats are shown in Figure 4A and B, respectively. $T_{app}$ in the trachea was obviously higher than that in the tissues in both healthy and COPD rats. Compared with the healthy rats, the $T_{app}$ distribution obviously increased in the COPD rats pulmonary parenchyma and was more inhomogeneous. Furthermore, the $T_{app}$ distribution in COPD rats (Figure 4D) shifted toward higher values compared with healthy rats (Figure 4C).

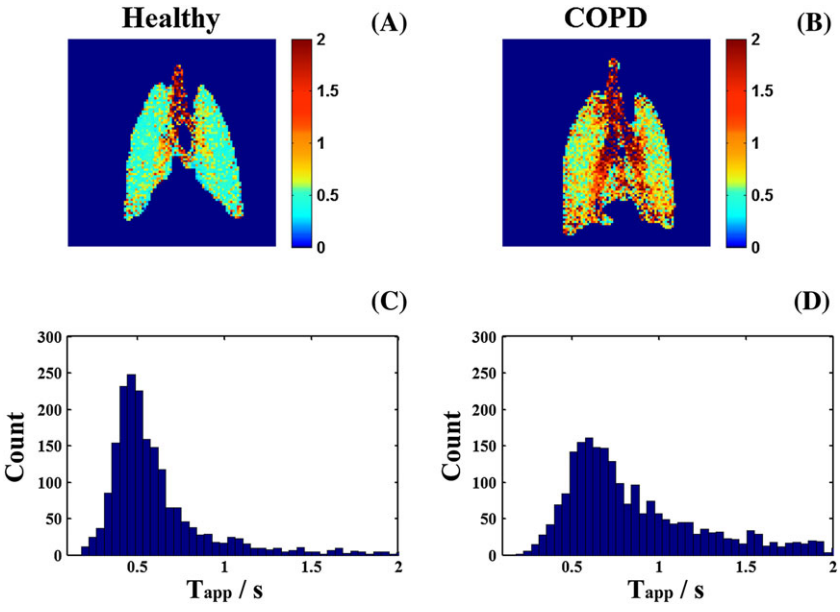


**FIGURE 4** The typical $T_{app}$ distributions acquired with 100 saturation pulses centered at 200 ppm in healthy rats and COPD rats by hyperpolarized $^{129}$Xe CEST MRI. The $T_{app}$ maps of healthy and COPD rats are shown in A and B, respectively. The histograms of the local $T_{app}$ over the lungs shifted towards higher values in the COPD rat (D) compared with the healthy rat (C), and the mean value of $T_{app}$ increased from 0.69 s to 1.06 s

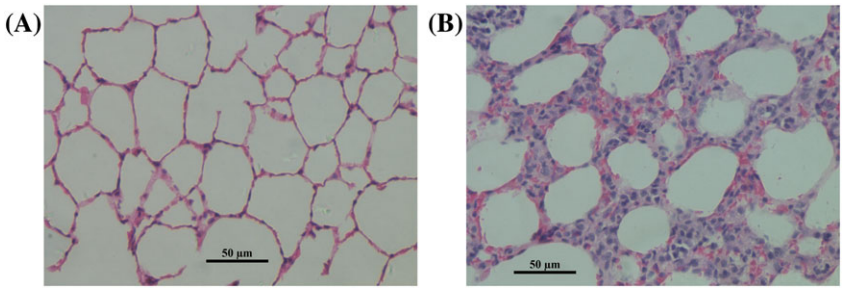


**FIGURE 5** Typical H&E-stained lung images of a healthy rat (A) and COPD rat (B). In the COPD rat, an accumulation of inflammatory cell infiltration was observed in the alveolar wall. Magnification= 40×

### 3.3 | Histology

As shown in Figure 5, interstitial alveolar wall thickening and accumulation of inflammatory cell infiltration were observed in the entire lung among COPD rats. The alveolar diameter in COPD rats obviously increased compared with the controls ($P$ = 0.005), and the mean alveolar diameters were 46.4 ± 2.9 μm and 40.1 ± 2.1 μm in COPD rats and healthy rats, respectively.

## 4 | DISCUSSION

In this study, a CEST sequence was employed to evaluate the pulmonary gas exchange function, and a new parameter, named the pulmonary apparent gas exchange time constant ($T_{app}$), was proposed to characterize the pulmonary gas exchange function. The measured $T_{app}$ values in healthy and COPD rats were 0.63 ± 0.06 s and 0.95 ± 0.14 s, respectively, with a significant difference ($P$ = 0.001) between the groups. The measured mean value of $T_{app}$ in COPD rats increased over that of the healthy group, mainly due to lung inflammation and enlargement of the alveoli caused by cigarette smoke and LPS exposure.[36,37] The histological results showed that the diameter of the alveoli measured in COPD rats obviously increased ($P$ = 0.005), from 40.1 ± 2.1 μm to 46.4 ± 2.9 μm compared with the control group, and that enlarged alveoli decreased the efficiency of gas transfer in the lungs of COPD rats. Additionally, obvious accumulation of inflammatory cell infiltration was observed in COPD rats, which may change the diffusion capacity of the alveolar wall and affect the measured $T_{app}$. Our results indicate that the proposed parameter ($T_{app}$), derived from CEST, can quantify changes in the pulmonary gas exchange function in vivo.

$T_{app}$ distributions in the lung showed a significant difference between healthy and COPD rats: $T_{app}$ in COPD rats was obviously larger than in healthy rats. The measured $T_{app}$ in the trachea was obviously larger than that in the parenchyma of both healthy and COPD rats, because gas exchange mostly occurs in the parenchyma and the efficiency of gas exchange in the trachea is very low. Consequently, the xenon gas signal had almost no attenuation in the trachea when the saturation pulses were applied, and similar results were also observed in a previous study using XTC.[11] However, in the pulmonary parenchyma zone, where gas exchange is continuously ongoing and dissolved xenon from tissue and blood exchanges with xenon gas in the alveoli, the xenon gas signal diminished when the saturation pulses were applied on the resonance of dissolved xenon. In COPD rats, the gas utilization of the alveoli decreased due to the impairment of the alveolar walls and the decreased SVR of the alveoli caused by cigarette smoke and LPS exposure. Therefore, $T_{app}$ increased in COPD rats compared with healthy rats.

Compared with the direct measurement method, i.e. CSSR, the CEST method has several obvious advantages. First, the requirement for spin polarization of xenon gas is not as strict as in CSSR, which makes it more accessible in the clinical setting. In the CSSR experiments, the observed signal is the dissolved xenon signal in the lung, which is only approximately 2% of the gas signal intensity.[24] Furthermore, the signal has a large full width at half maximum (FWHM) because of the alveolar structure.[38] In the CEST experiments, the observed signal is from the xenon gas phase and the requirement for the signal intensity is low. Based on our experience regarding these experiments, global $T_{app}$ can be obtained accurately using hyperpolarized xenon CEST MR even if the SNR of the gaseous xenon signal is lower than 200 in the lung.

The pulse sequence of CEST is somewhat similar to XTC, as proposed by Ruppert et al., and both of the methods utilize the xenon gas signal to indirectly obtain the dynamics of the dissolved xenon signal.[11] However, XTC was intended to measure the gas exchange process in the lung and time between the saturation RF pulses,i.e., the exchange time was variable. By contrast, the method used in our study, CEST, was intended to evaluate the alveolar gas exchange capacity and the time between the saturation pulses was constant, so the dynamics of the xenon gas signal were measured by varying the number of saturation pulses, i.e. the saturation time.

Compared with the commonly used CEST sequence, a series of saturation RF pulses rather than a continuous waves (CW) are employed to saturate the signal, because the FWHM of the dissolved xenon signal in the lung is generally larger than 10 ppm,[38] and the CW cannot completely saturate the dissolved xenon signal. The ideal saturation is continuously destroying the dissolved xenon signal without any delays. However, to dephase the residual magnetism in the $x$-$y$ plane, a spoiler gradient pulse was added. Additionally, a 1 ms delay was added to perform the sequence because of the scanner's limitation in this study.

The CEST sequence used in our study was carefully designed to eliminate the signal's fluctuation and measure the actual xenon gas signal dynamics versus saturation time through exchange with dissolved xenon in the lung. Before data acquisition, an excitation pulse ($\alpha_1$) was applied to generate a reference signal for calibration to eliminate the effect of the signal's fluctuation during each breath, which was mainly from the relaxation of $^{129}$Xe gas in the Tedlar bag and the difference in the inhaling $^{129}$Xe gas volume caused by the precision of the gas delivery system, and the results from the control experiment showed the necessity of this subtle calibration. To avoid the influence of relaxation in the lung, the time between the two excitation pulses was set to the same value, 3 s in the spectroscopy experiments. Before the data were fitted to Equation (1), the xenon signal intensity was normalized by the control experiment, in which the saturation pulse was centered at −200 ppm to eliminate the effect of the flip angle in different rats. The acquired xenon gas signal in the control experiments was almost invariable with increasing saturation time when the saturation pulses were centered at −200 ppm, indicating that the pulse sequence satisfied the requirements of the experiments. Furthermore, the fitting in healthy and COPD rats showed goodness of fit and the *R*-square was greater than 0.95.

The goal of this work was to present a proof-of-concept study that investigates whether CEST MR has the potential to quantify the pulmonary gas exchange function. Some limitations existed in this work. First, only the gas exchange function was quantitatively evaluated, and corresponding theoretical models remain to be developed to extract the quantitative pulmonary structure information, which would be helpful for deep understanding of pulmonary gas exchange. Second, in the image experiments, only one time-point of gas exchange was utilized. To obtain the sophisticated gas exchange function, experiments with multiple time-points of gas exchange are needed. Meanwhile, acquisition was accomplished in separate breaths, but for clinical applications a faster method is expected to acquire data within a single breath-hold.[22,23,25] The third limitation was the inherent limitation of the CEST sequence. The dissolved xenon signals in the tissue and blood contained some information about pulmonary gas exchange, and some useful information can be obtained by subtly analyzing the dissolved xenon signals in tissue and blood to characterize pulmonary diseases.[38,39] However, in the method of CEST, the dissolved xenon signals in tissue and blood were treated as a single unit, causing a potential loss of valuable information. Another limitation of this study was the use of animal models. The COPD model was induced by cigarette smoke exposure, and LPS was used to accelerate the process of modeling. $T_{app}$ showed an obvious difference between the model and control groups. However, the model was not perfect for the proposed method, because both cigarette smoke exposure and LPS will induce lung inflammation, and this inflammation will change the radius of the alveoli,[40] which may influence the apparent gas exchange efficient. Additionally, long-term cigarette smoke exposure will enlarge the alveoli. An appropriate animal model characterized by an alteration of only the radius of the alveoli or only the diffusion capacity of the alveolar gas-exchange membrane will be helpful in the future.

## 5 | CONCLUSION

In this study, we demonstrated the feasibility of hyperpolarized $^{129}$Xe CEST MRI for evaluating the pulmonary gas exchange function and proposed a new parameter, $T_{app}$, to quantitatively characterize the lung gas exchange function. $T_{app}$ showed a significant difference between COPD and healthy rats and increased in the pulmonary parenchyma of COPD rats compared with healthy rats. Our results indicate that $T_{app}$ can be used to quantitatively evaluate the gas exchange efficiency of the lung, which would be helpful for the diagnosis of lung diseases that are related to gas exchange.

### ACKNOWLEDGEMENTS

This work was supported by the National Key R&D Program of China (2016YFC1304700 and 2017YFA0505400), National Natural Science Foundation of China (81625011, 81227902, and 81601491), and Key Research Program of Frontier Sciences, CAS (QYZDY-SSW-SLH018). XZ acknowledges support by the National Program for Support of Eminent Professionals (National Program for Support of Top-Notch Young Professionals).

### ORCID

*Xin Zhou* http://orcid.org/0000-0002-5580-7907

### REFERENCES

1. Albert MS, Cates GD, Driehuys B, et al. Biological magnetic resonance imaging using laser-polarized Xe-129. *Nature*. 1994;370:199-201.
2. Mansson S, Wolber J, Driehuys B, Wollmer P, Golman K. Characterization of diffusing capacity and perfusion of the rat lung in a lipopolysaccaride disease model using hyperpolarized Xe-129. *Magn Reson Med*. 2003;50:1170-1179.
3. Driehuys B, Cofer GP, Pollaro J, et al. Imaging alveolar-capillary gas transfer using hyperpolarized Xe-129 MRI. *Proc Natl Acad Sci U S A*. 2006;103:18278-18283.
4. Mugler JP, Altes TA, Ruset IC, et al. Simultaneous magnetic resonance imaging of ventilation distribution and gas uptake in the human lung using hyperpolarized xenon-129. *Proc Natl Acad Sci U S A*. 2010;107:21707-21712.
5. Walker TG, Happer W. Spin-exchange optical pumping of noble-gas nuclei. *Rev Mod Phys*. 1997;69:629-642.

6. Pavlovskaya GE, Cleveland ZI, Stupic KF, Basaraba RJ, Meersmann T. Hyperpolarized krypton-83 as a contrast agent for magnetic resonance imaging. *Proc Natl Acad Sci U S A*. 2005;102:18275-18279.
7. Yablonskiy DA, Sukstanskii AL, Leawoods JC, et al. Quantitative in vivo assessment of lung microstructure at the alveolar level with hyperpolarized $^{3}$He diffusion MRI. *Proc Natl Acad Sci U S A*. 2002;99:3111-3116.
8. Miller KW, Reo NV, Uiterkamp AS, et al. Xenon NMR: chemical shifts of a general anesthetic in common solvents, proteins, and membranes. *Proc Natl Acad Sci U S A*. 1981;78:4946-4949.
9. Stewart NJ, Leung G, Norquay G, et al. Experimental validation of the hyperpolarized $^{129}$Xe chemical shift saturation recovery technique in healthy volunteers and subjects with interstitial lung disease. *Magn Reson Med*. 2015;74:196-207.
10. Chang YV, Quirk JD, Ruset IC, et al. Quantification of human lung structure and physiology using hyperpolarized Xe-129. *Magn Reson Med*. 2014;71:339-344.
11. Ruppert K, Brookeman JR, Hagspiel KD, Mugler JP. Probing lung physiology with xenon polarization transfer contrast (XTC). *Magn Reson Med*. 2000;44:349-357.
12. Patz S, Muradyan I, Hrovat MI, et al. Diffusion of hyperpolarized Xe-129 in the lung: a simplified model of Xe-129 septal uptake and experimental results. *New J Phys*. 2011;13:015009.
13. Qing K, Mugler JP, Altes TA, et al. Assessment of lung function in asthma and COPD using hyperpolarized $^{129}$Xe chemical shift saturation recovery spectroscopy and dissolved-phase MRI. *NMR Biomed*. 2014;27:1490-1501.
14. Ruppert K, Mata JF, Brookeman JR, Hagspiel KD, Mugler JP. Exploring lung function with hyperpolarized Xe-129 nuclear magnetic resonance. *Magn Reson Med*. 2004;51:676-687.
15. Ruppert K, Mata JF, H-TJ W, et al. XTC MRI: sensitivity improvement through parameter optimization. *Magn Reson Med*. 2007;57:1099-1109.
16. Chang YV. MOXE: a model of gas exchange for hyperpolarized $^{129}$Xe magnetic resonance of the lung. *Magn Reson Med*. 2013;69:884-890.
17. Dregely I, Ruset IC, Mata JF, et al. Multiple-exchange-time xenon polarization transfer contrast (MXTC) MRI: initial results in animals and healthy volunteers. *Magn Reson Med*. 2012;67:943-953.
18. Dregely I, Mugler JP, Ruset IC, et al. Hyperpolarized xenon-129 gas-exchange imaging of lung microstructure: first case studies in subjects with obstructive lung disease. *J Magn Reson Imaging*. 2011;33:1052-1062.
19. Santyr G, Fox M, Thind K, et al. Anatomical, functional and metabolic imaging of radiation-induced lung injury using hyperpolarized MRI. *NMR Biomed*. 2014;27:1515-1524.
20. Li H, Zhang Z, Zhao X, et al. Quantitative evaluation of radiation-induced lung injury with hyperpolarized xenon magnetic resonance. *Magn Reson Med*. 2016;76:408-416.
21. Stewart NJ, Horn FC, Norquay G, et al. Reproducibility of quantitative indices of lung function and microstructure from $^{129}$Xe chemical shift saturation recovery (CSSR) MR spectroscopy. *Magn Reson Med*. 2017;77:2107-2113.
22. Kaushik SS, Robertson SH, Freeman MS, et al. Single-breath clinical imaging of hyperpolarized $^{129}$Xe in the airspaces, barrier, and red blood cells using an interleaved 3D radial 1-point Dixon acquisition. *Magn Reson Med*. 2015;75:1434-1443.
23. Qing K, Ruppert K, Jiang Y, et al. Regional mapping of gas uptake by blood and tissue in the human lung using hyperpolarized xenon-129 MRI. *J Magn Reson Imaging*. 2014;39:346-359.
24. Ruppert K, Brookeman JR, Hagspiel KD, Driehuys B, Mugler JP. NMR of hyperpolarized $^{129}$Xe in the canine chest: spectral dynamics during a breath-hold. *NMR Biomed*. 2000;13:220-228.
25. Muradyan I, Butler JP, Dabaghyan M, et al. Single-breath xenon polarization transfer contrast (SB-XTC): implementation and initial results in healthy humans. *J Magn Reson Imaging*. 2013;37:457-470.
26. Schröder L, Lowery TJ, Hilty C, Wemmer DE, Pines A. Molecular imaging using a targeted magnetic resonance hyperpolarized biosensor. *Science*. 2006;314:446-449.
27. Gomes MD, Dao P, Jeong K, et al. $^{129}$Xe NMR relaxation-based macromolecular sensing. *J Am Chem Soc*. 2016;138:9747-9750.
28. Riggle BA, Wang Y, Dmochowski IJ. A "smart" $^{129}$Xe NMR biosensor for pH-dependent cell labeling. *J Am Chem Soc*. 2015;137:5542-5548.
29. Zhou X. Hyperpolarized noble gases as contrast agents. In: Schröder L, Faber C, eds. *In vivo NMR Imaging*. New York City, New York: Humana Press; 2011:189-204.
30. Ruan W, Zhong J, Wang K, et al. Detection of the mild emphysema by quantification of lung respiratory airways with hyperpolarized xenon diffusion MRI. *J Magn Reson Imaging*. 2017;45:879-888.
31. Li H, Zhang Z, Zhong J, et al. Oxygen-dependent hyperpolarized $^{129}$Xe brain MR. *NMR Biomed*. 2016;29:220-225.
32. Nouls J, Fanarjian M, Hedlund L, Driehuys B. A constant-volume ventilator and gas recapture system for hyperpolarized gas MRI of mouse and rat lungs. *Concepts Magn Reson B*. 2011;39B:78-88.
33. Deng H, Zhong J, Ruan W, et al. Constant-variable flip angles for hyperpolarized media MRI. *J Magn Reson*. 2016;263:92-100.
34. Zhong J, Ruan W, Han Y, et al. Fast determination of flip angle and $T_1$ in hyperpolarized gas MRI during a single breath-hold. *Sci Rep*. 2016;6:25854.
35. Ji M, Wang Y, Li X, Qian Z. Up-regulation of ICAM-1mRNA and IL-1βmRNA in lung tissues of a rat model of COPD. *Int J Clin Exp Med*. 2015;8:21956-21963.
36. Hardaker EL, Freeman MS, Dale N, et al. Exposing rodents to a combination of tobacco smoke and lipopolysaccharide results in an exaggerated inflammatory response in the lung. *Br Pharmacol*. 2010;160:1985-1996.
37. Nie Y-C, Wu H, Li P-B, et al. Characteristic comparison of three rat models induced by cigarette smoke or combined with LPS: to establish a suitable model for study of airway mucus hypersecretion in chronic obstructive pulmonary disease. *Pulm Pharmacol Ther*. 2012;25:349-356.
38. Robertson SH, Virgincar RS, Bier EA, et al. Uncovering a third dissolved-phase $^{129}$Xe resonance in the human lung: quantifying spectroscopic features in healthy subjects and patients with idiopathic pulmonary fibrosis. *Magn Reson Med*. 2017;78:1306-1315.
39. Virgincar RS, Robertson SH, Nouls J, et al. Establishing an accurate gas phase reference frequency to quantify $^{129}$Xe chemical shifts in vivo. *Magn Reson Med*. 2017;77:1438-1445.

40. Ouriadov A, Fox M, Hegarty E, et al. Early stage radiation-induced lung injury detected using hyperpolarized $^{129}$Xe morphometry: proof-of-concept demonstration in a rat model. *Magn Reson Med*. 2016;75:2421-2431.

**How to cite this article:** Li H, Zhang Z, Zhao X, et al. Quantitative evaluation of pulmonary gas-exchange function using hyperpolarized $^{129}$Xe CEST MRS and MRI. *NMR in Biomedicine*. 2018;31:e3961. https://doi.org/10.1002/nbm.3961